# CEP290 tethers flagellar transition zone microtubules to the membrane and regulates flagellar protein content

Branch Craige,[1] Che-Chia Tsao,[2] Dennis R. Diener,[2] Yuqing Hou,[1] Karl-Ferdinand Lechtreck,[1] Joel L. Rosenbaum,[2] and George B. Witman[1]

[1]Department of Cell Biology, University of Massachusetts Medical School, Worcester, MA 01655
[2]Department of Molecular, Cellular and Developmental Biology, Yale University, New Haven, CT 06520

Mutations in human *CEP290* cause cilia-related disorders that range in severity from isolated blindness to perinatal lethality. Here, we describe a *Chlamydomonas reinhardtii* mutant in which most of the *CEP290* gene is deleted. Immunoelectron microscopy indicated that CEP290 is located in the flagellar transition zone in close association with the prominent microtubule–membrane links there. Ultrastructural analysis revealed defects in these microtubule–membrane connectors, resulting in loss of attachment of the flagellar membrane to the transition zone microtubules. Biochemical analysis of isolated flagella revealed that the mutant flagella have abnormal protein content, including abnormal levels of intraflagellar transport proteins and proteins associated with ciliopathies. Experiments with dikaryons showed that CEP290 at the transition zone is dynamic and undergoes rapid turnover. The results indicate that CEP290 is required to form microtubule–membrane linkers that tether the flagellar membrane to the transition zone microtubules, and is essential for controlling flagellar protein composition.

## Introduction

Mutations that disrupt the assembly, structure, and/or function of cilia or flagella result in cilia-related disorders termed ciliopathies (Badano et al., 2006; Fliegauf et al., 2007). Mutations in *CEP290* cause ciliopathies that exhibit a range of severity (Helou et al., 2007). *CEP290* mutations are a common cause of Leber congenital amaurosis (LCA; den Hollander et al., 2006; Sundaresan et al., 2009), in which blindness results from degeneration of the retina but other organ systems are often unaffected. Other *CEP290* mutations cause Meckel syndrome (Baala et al., 2007; Frank et al., 2008), a perinatal-lethal disease in which essentially all tissues with cilia are affected. Of intermediate severity is Joubert syndrome, in which brain development is affected and which often also presents with ocular and renal manifestations (Sayer et al., 2006; Valente et al., 2006; Brancati et al., 2007).

The described subcellular localization of CEP290 (also known as nephrocystin-6/NPHP6) is consistent with a role for CEP290 in cilia. In mammalian cells, CEP290 has been localized to centrosomes/basal bodies (Andersen et al., 2003; Chang et al., 2006; Sayer et al., 2006; Valente et al., 2006; Tsang et al., 2008), pericentriolar satellites (Kim et al., 2008), the connecting cilium of photoreceptors (Chang et al., 2006; Sayer et al., 2006), and the dendritic knobs of olfactory sensory neurons (McEwen et al., 2007), and CEP290 was immunoprecipitated with centrosomal components (Chang et al., 2006; McEwen et al., 2007; Tsang et al., 2008). CEP290 has a nuclear localization signal and, in addition to its cytoplasmic localization, has been observed in the nucleus (Guo et al., 2004; Sayer et al., 2006).

The exact role of CEP290 is unclear, but all available evidence suggests that CEP290 is somehow involved in ciliary function. Morpholino knockdown of CEP290 in zebrafish resulted in retinal, renal, and cerebellar phenotypes that are indicative of defects in cilia and are commonly seen in humans with Joubert syndrome (Sayer et al., 2006). Defects in the localization of several ciliary proteins were found in photoreceptors and

Correspondence to George B. Witman: George.Witman@umassmed.edu

Abbreviations used in this paper: BAC, bacterial artificial chromosome; BBS, Bardet-Biedl syndrome; DIC, differential interference contrast; IFT, intraflagellar transport; LCA, Leber congenital amaurosis.



The Rockefeller University Press $30.00
J. Cell Biol. Vol. 190 No. 5 927–940
www.jcb.org/cgi/doi/10.1083/jcb.201006105

olfactory sensory neurons of the *rd16* mouse, which harbors a hypomorphic in-frame deletion in *Cep290* and displays early-onset retinal degeneration and anosmia (Chang et al., 2006; McEwen et al., 2007). In addition, RNAi knockdown of CEP290 in cultured mammalian cells decreased the percentage of cells displaying primary cilia (Graser et al., 2007; Tsang et al., 2008). CEP290 binds to and activates the transcription factor ATF4, a protein implicated in renal cyst formation (Sayer et al., 2006). Collectively, the data suggest that CEP290 is involved in ciliary assembly and the expression, targeting, or transport of ciliary proteins, but why CEP290 deficiency causes defects in cilia is unknown.

To elucidate the molecular role of CEP290, we used *Chlamydomonas reinhardtii*, which has numerous characteristics that make it an ideal model organism for studying the function of ciliary and basal body components. Human and *C. reinhardtii* CEP290 are highly conserved (Basic Local Alignment Search Tool [BLAST] E = 5 e−27); Keller et al. (2005) previously identified the *C. reinhardtii* CEP290 orthologue by proteomic analysis of isolated centrioles. Our results show that *C. reinhardtii* CEP290 is localized to the transition zone between the flagellar basal body and axoneme, where it is required for the assembly of the microtubule–membrane linkers characteristic of this poorly understood region. Loss of the protein results in defects in flagellar composition, including alteration of the normal balance of intraflagellar transport (IFT) complexes A and B and abnormal levels of the membrane-associated proteins BBS4 and PKD2, the human homologues of which are involved in ciliopathies. The results also show that CEP290 is highly dynamic at the transition zone, which suggests that it may be involved in signaling between the cilium and cell body, and which has clinical implications for *CEP290* gene therapy in the retina to treat LCA due to defects in *CEP290*. We propose that CEP290 is part of a complex that links the membrane to the microtubules in the transition zone and regulates entry of proteins into the ciliary compartment.

## Results

### Identification of a *C. reinhardtii cep290* mutant

To understand how CEP290 deficiency affects flagellar function, a library of *C. reinhardtii* insertional mutants was screened using PCR with primers complementary to sequences in the 5′ and 3′ regions of the *C. reinhardtii CEP290* homologue (previously designated *POC3*; Keller et al., 2005). In one strain (Y168), primers directed toward the 3′ end of *CEP290* failed to amplify a product, which indicated that this region is deleted (Fig. 1 A). Further analysis by PCR revealed an ∼18.5-kb deletion encompassing all but the first 2–4 exons (out of a total of 37 exons) of *CEP290*. The mutant cells were mostly palmelloid (i.e., failed to hatch from the mother cell wall after mitosis; Fig. 1 B). Release from the mother cell wall by treatment with autolysin enzyme (Harris, 2009) demonstrated that the cells have very short/stumpy flagella, some of which begin to elongate over time (Fig. 1 C). Occasionally, bulges were present in the short or stumpy mutant flagella (Fig. 1 D).

The Y168 mutant was backcrossed twice to wild-type cells (the F2 progeny with the deletion is henceforth referred to as *cep290*), and each time the mutant phenotype cosegregated with the deletion. The mutant phenotype was rescued by transformation with genomic DNA encoding either untagged or HA-tagged CEP290 and no other gene (Fig. 1, A and B; and Videos 1–4), which confirmed that the mutant phenotype is caused by the deletion of *CEP290*. Antibodies generated against a peptide consisting of the last 14 amino acids in the C terminus of *C. reinhardtii* CEP290 recognized a single band of the predicted molecular mass (275 kD) that was present in Western blots of whole-cell lysates of wild-type and rescued cells, but absent in *cep290* cells, which confirmed that the antibody is specific and that CEP290 is absent in the mutant (Fig. 1 E).

### CEP290 is located in the transition zone

Immunofluorescence microscopy using the antibody directed against CEP290 showed CEP290 immunoreactivity at the base of each flagellum of wild-type cells (Fig. 2 A, a–c; and Fig. 2 B); the label was missing from *cep290* mutant cells (Fig. 2 A, d–f), indicating that the labeling was specific. This localization pattern was confirmed by using the CEP290-HA rescued strain and antibodies to HA (see Fig. 6). Co-labeling with antibodies to polyglutamylated tubulin, which label basal bodies and flagellar axonemes but fail to label the transition zone of flagella (Lechtreck and Geimer, 2000), revealed that the CEP290 signal was located in the region that lacked polyglutamylated tubulin labeling, indicating that CEP290 is located in the transition zone (Fig. 2 C). CEP290 remained associated with the transition zone after deflagellation (Fig. S1), a finding that is consistent with its presence in the *C. reinhardtii* centriole proteome (which included the transition zone; Keller et al., 2005) and its absence in the *C. reinhardtii* flagellar proteome (which lacked the transition zone; Pazour et al., 2005). CEP290 was undetectable in Western blots of isolated flagella (Fig. S2), which confirmed that CEP290 does not enter the flagellar compartment distal to the transition zone.

### *cep290* mutant cells have defects in the structures that bridge the transition zone microtubules and membrane

To determine if loss of CEP290 resulted in ultrastructural defects, we examined *cep290* mutant cells by EM. We observed no defects in basal bodies. In longitudinal sections through the transition zone, the wedge-shaped structures that extend between the doublet microtubules and membrane in wild-type cells (Ringo, 1967) were missing or collapsed onto the doublets in the mutant cells (Fig. 3, A and B). In cross sections through transition zones, the Y-shaped connectors that extend from the transition zone doublet microtubules to the flagellar membrane were often absent in the mutant cells (Fig. 3, C and D). Image averaging (Fig. 3, C and D, insets) revealed remnants of Y connectors on the mutant doublets, including a small electron density possibly corresponding to the base of the Y connector. In short flagella, we occasionally observed bulges in the flagellar membrane filled with electron-dense material (Fig. 3, E–G). In rare instances, we observed defects in axonemal microtubules (Fig. 3 F); however, the vast majority of sections

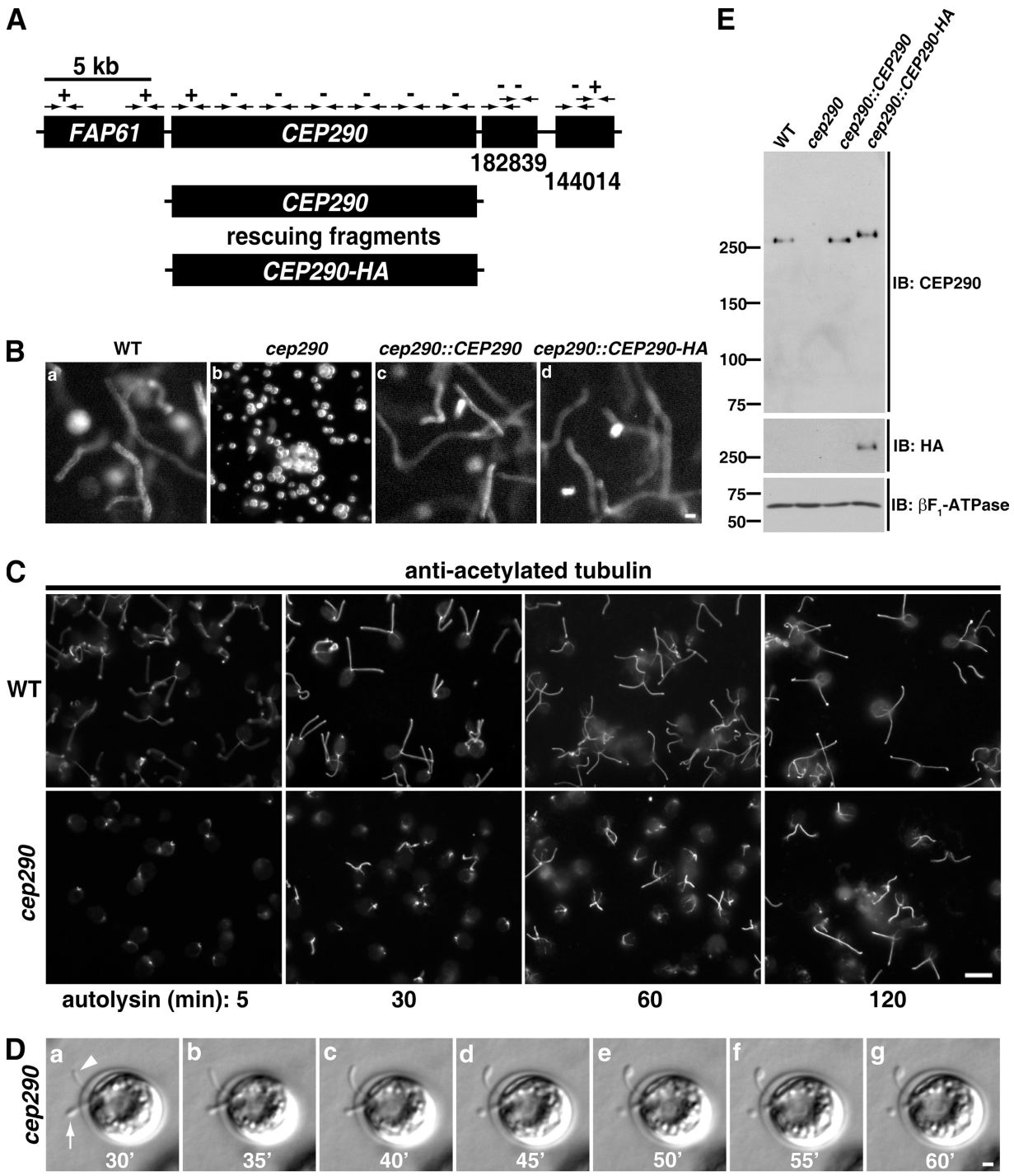


Figure 1. **Identification of a *C. reinhardtii* CEP290 mutant.** (A) Schematic of the region of *C. reinhardtii* chromosome 3 containing the *CEP290* (*POC3*) locus. *CEP290* is flanked by the *FAP61* gene and by gene models encoding predicted proteins nos.182839 and 144014 in Joint Genome Institute version 4.0 of the *Chlamydomonas* genome (http://genome.jgi-psf.org/Chlre4/Chlre4.home.html). Arrows indicate the positions of PCR primer pairs; plus and minus symbols indicate whether a PCR product was generated using genomic DNA of strain Y168 as template (all primer pairs amplified a product when wild-type genomic DNA was used as template). Rescuing constructs consisted of either untagged or HA-tagged genomic DNA fragments containing only the *CEP290* gene. (B) 30-frame image averages of videos (acquired at 30 frames per second) depicting the mutant phenotype (*cep290*) and rescue of the phenotype (*cep290::CEP290* and *cep290::CEP290-HA*). Motile cells are seen as long meandering tracks, whereas nonmotile (palmelloid) cells appear as bright foci (*cep290*). See Videos 1–4. Bar, 10 μm. (C) Palmelloid *cep290* mutant cells were released from the mother cell wall by treatment with autolysin, then fixed at the indicated time points after the addition of autolysin and processed for immunofluorescence using antibodies to acetylated tubulin. The mutant cells have stumpy flagella that partially elongate over time. Bar, 10 μm. (D) *cep290* mutant cells were hatched with autolysin, immobilized in 0.5% agar, and imaged at the indicated time points (minutes) after the addition of autolysin. The arrowhead marks a flagellum that began to elongate then formed a bulge. The arrow marks a flagellum that failed to elongate and formed a bulge. Bar, 1 μm. (E) Western blot of whole cells. A peptide antibody generated against the C-terminal 14 amino acids of *C. reinhardtii* CEP290 is specific and confirms the absence of CEP290 in the mutant strain and expression of CEP290 in the rescued strains. βF1-ATPase is a mitochondrial protein used as a loading control. The positions of standard proteins and their molecular masses in kD are indicated.

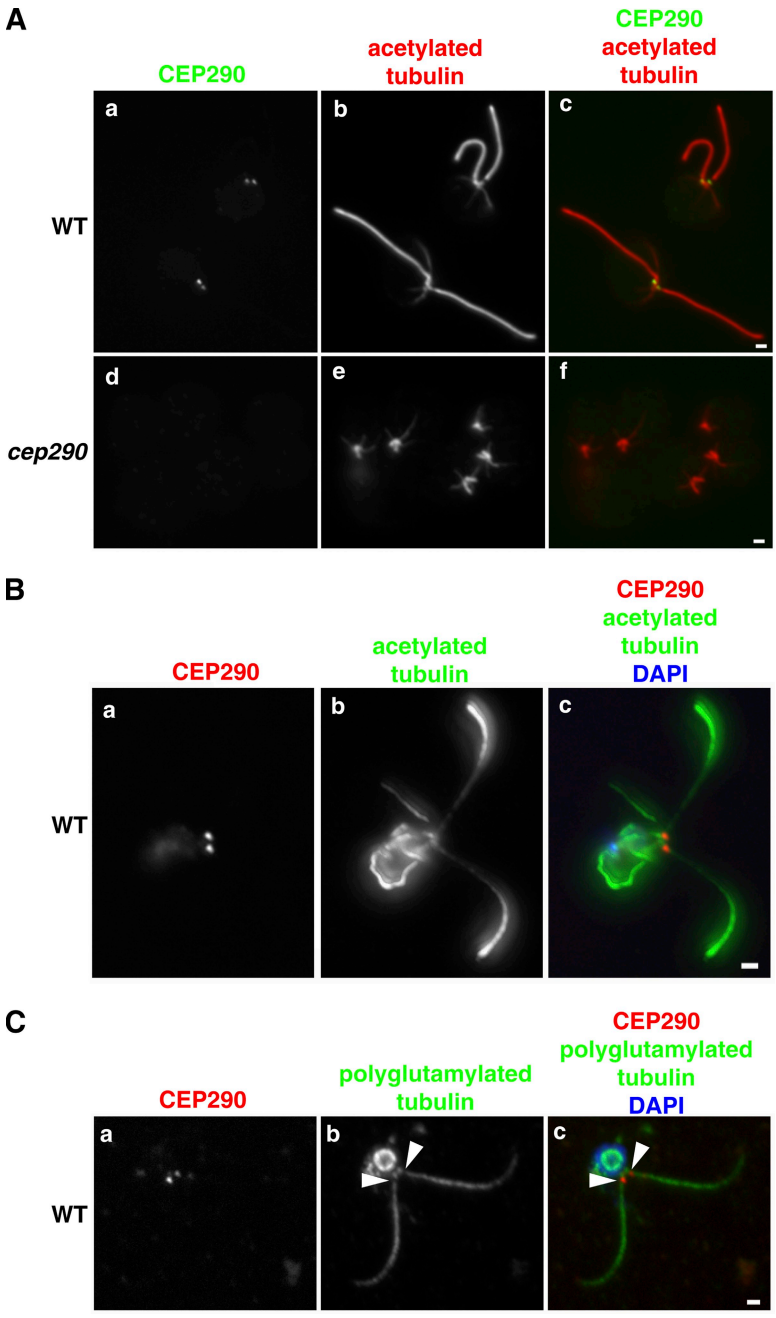


Figure 2. ***C. reinhardtii* CEP290 is located in the transition zone.** (A) Wild-type and *cep290* mutant cells were fixed and processed for immunofluorescence using the indicated antibodies. (B and C) Wild-type cells were detergent-extracted, and the resulting cytoskeletons were processed for immunofluorescence using the indicated antibodies. Co-labeling with antibodies to CEP290 and acetylated tubulin revealed CEP290 localization at the base of each flagellum (A and B). (C) Co-labeling with polyglutamylated tubulin indicated that CEP290 is located within the transition zone (arrowheads; Lechtreck and Geimer, 2000). Also see Fig. S1. Bars, 1 µm.

through axonemes revealed normal outer doublets, radial spokes, dynein arms, and central pair microtubules.

To determine if the disruption of the transition zone structures altered the normal relationship between the transition zone microtubules and membrane, we measured the distance between the transition zone cylinder and the membrane in wild-type and mutant cells. In *cep290* mutant cells, the distance was greater and more variable (Fig. 3 H). To determine if this reflects a functional detachment of the membrane from the microtubules, we examined the association of the transition zone membrane with the underlying microtubules in detergent-extracted cytoskeletons. In wild-type cells, the transition zone membrane remains intact and associated with the transition zone microtubules after detergent extraction (Fig. 3 I; Kamiya and Witman, 1984). In contrast, in the mutant, the transition zone membrane was lost after detergent extraction (Fig. 3 J). The data indicate that loss of CEP290 causes defects in the microtubule–membrane connections in the transition zone, which results in loss of attachment of the flagellar membrane to the transition zone.

### CEP290 localizes to the transition zone microtubule–membrane connectors

Single- and double-label immunogold EM was used to localize CEP290 more precisely within the transition zone. Using the antibody that recognizes the C-terminal 14 amino acids of CEP290, gold particles exclusively labeled the transition zone of detergent-extracted cytoskeletons of wild-type cells, with most labeling between the doublet microtubules and the membrane (Fig. 4, A–C;

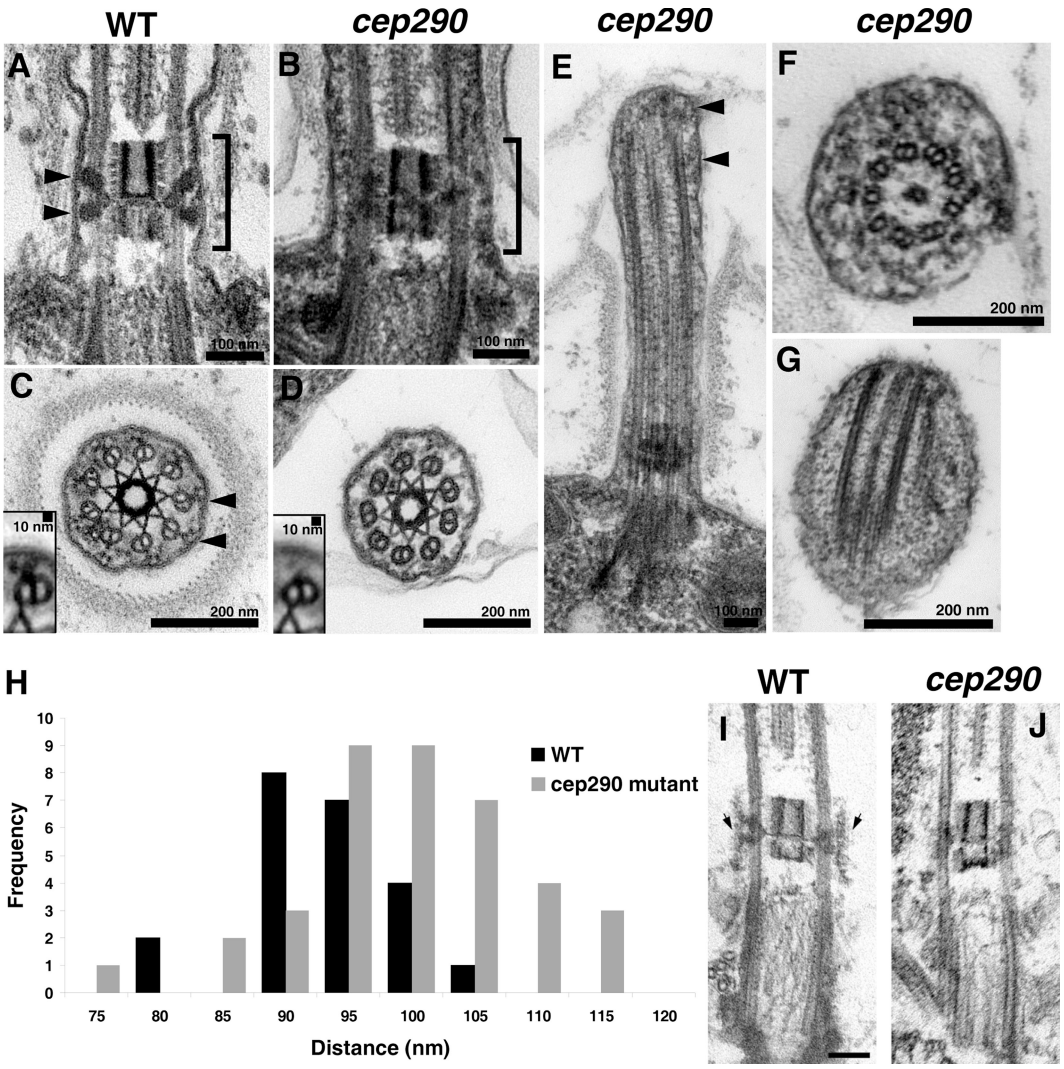


Figure 3. **Loss of CEP290 causes defects in the microtubule–membrane connections within the transition zone.** (A and B) Longitudinal sections through the transition zone (brackets) reveal that the electron-dense wedge-shaped structures (arrowheads in A) between the transition zone microtubules and flagellar membrane are missing in the *cep290* mutant. (C and D) Cross sections reveal that the Y-shaped connectors (arrowheads in C) that bridge the transition zone microtubules with the membrane are missing from most *cep290* doublet microtubules. Insets in C and D are image averages of 30 transition zone doublet microtubules. (E–G) Some of the mutant flagella have bulges filled with electron-dense material (arrowheads in E). The flagellum shown in F also has defects in axonemal doublets and the central pair microtubules; however, such defects are unusual in the mutant, as most axonemal cross sections appear normal. (H) Histogram depicting the distribution of the distances between the transition zone cylinder and the flagellar membrane in wild-type and *cep290* mutant cells; the difference in the distributions is significant at P = 0.0025 for a Student's *t* test and P = 0.0009 for a Welch's *t* test. (I and J) Cells were detergent-extracted, then fixed and processed for EM. The detergent-resistant membrane that remains attached to the wild-type transition zone (arrows in I) is no longer attached to the mutant transition zone. Bar, 100 nm.

Fig. S3, and Fig. S4). In longitudinal sections, gold particles were distributed throughout the length of the transition zone, with the highest concentration in the proximal part of the transition zone. In cross sections, most gold particles were located in the space between the Y-shaped connectors, with a few over the connectors. No labeling was observed with cytoskeletons of *cep290* mutant cells treated in an identical manner (Fig. S3, A–D). Using antibodies to the HA epitope, which is located near the middle of CEP290-HA (Fig. 4 D), and cells that were rescued with the tagged protein, we again observed a concentration of gold particles between the transition zone doublet microtubules and membrane. In this case, they were centered longitudinally in the transition zone, close to or over the wedge-shaped structures (Figs. 4 B and S4). In cross sections, the gold particles labeled the Y connectors and the area immediately surrounding the Y connectors (Figs. 4 C and S4). These experiments confirm that CEP290 is located in the transition zone, and suggest that the middle of CEP290 is closely associated with the microtubule–membrane connectors in the center of that region, whereas the C terminus of the protein is slightly more dispersed. These results are consistent with our ultrastructural findings that these connectors are missing or altered in the mutant.

### *cep290* mutant flagella have an abnormal protein composition

An important advantage of *C. reinhardtii* is that the flagella can be isolated, so that the effect of loss of CEP290 on flagellar protein content can be assessed biochemically. Flagella were

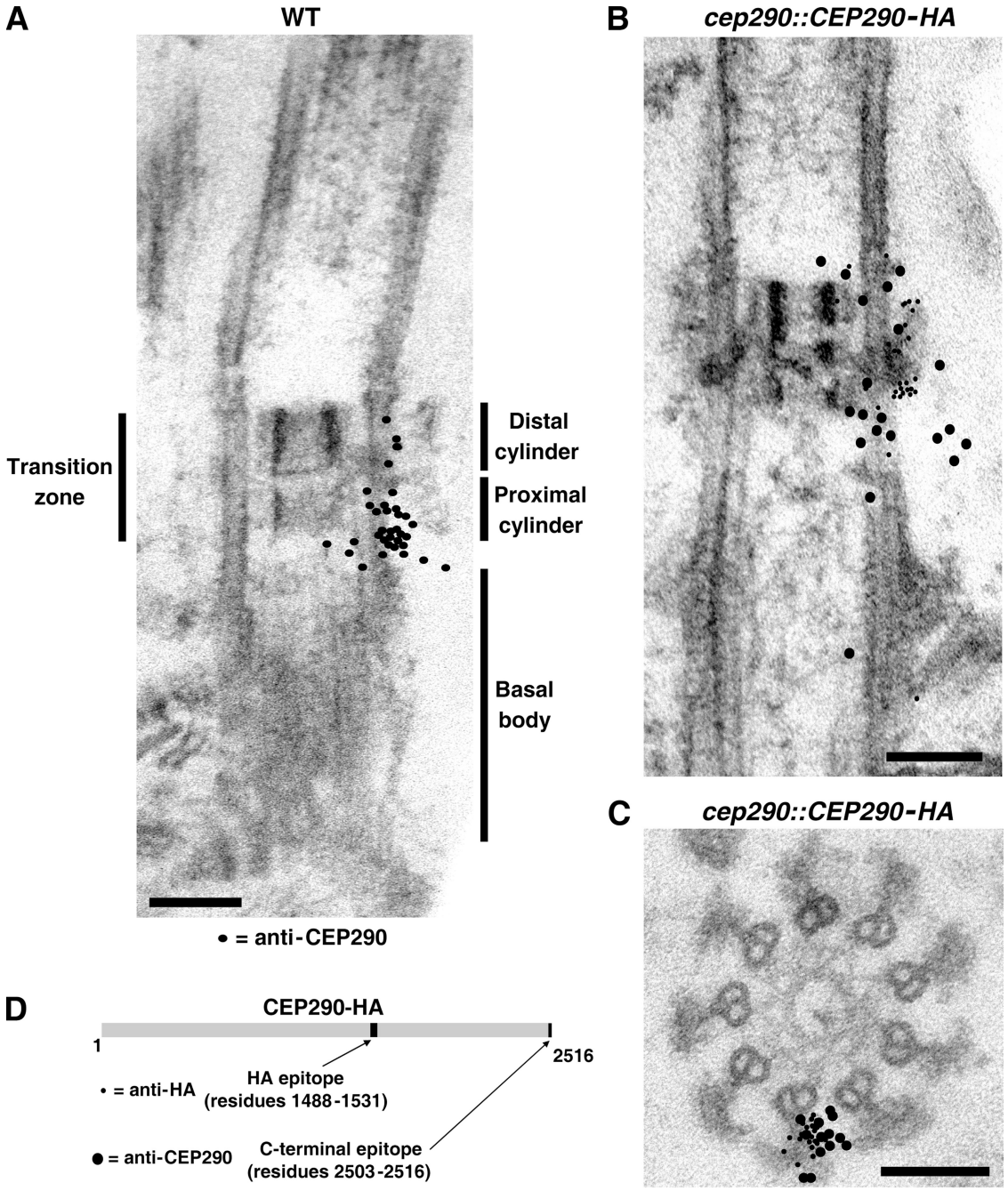


Figure 4. **Immunogold localization of CEP290.** (A) Wild-type detergent-extracted cytoskeletons were incubated with CEP290 antibody and gold-conjugated secondary antibody, then fixed, embedded, and sectioned. The locations of 34 gold particles from ~30 sections are indicated by black dots superimposed on the EM. For simplicity, the black dots are depicted on only one side of the transition zone; no bias for either side of the transition zone was observed. A selection of original micrographs is shown in Fig. S3. (B and C) *cep290::CEP290-HA* cytoskeletons were double-labeled with antibodies to CEP290 (12-nm gold) and HA (6-nm gold). As in A, the locations of the particles from several longitudinal sections (B) and cross sections (C) are represented by black dots superimposed on a single EM. A selection of original micrographs is shown in Fig. S4. Bars, 100 nm. (D) Schematic of HA-tagged CEP290 depicting the locations of the HA and C-terminal epitopes.

isolated from wild-type and *cep290* mutant cells, and their proteins were compared in Western blots and silver-stained gels. The mutant flagella had increased amounts of IFT complex B proteins and BBS4 relative to wild-type flagella, and decreased amounts of the IFT complex A protein IFT139 and polycystin-2 (Fig. 5 A). Comparison of wild-type and mutant flagella in silver-stained gels, followed by mass spectrometry to identify selected bands, revealed that some proteins, including EF-3 and EF1-α, were abnormally increased, whereas other proteins, including flagellar adenylate kinase, FAP5 (conserved uncharacterized flagellar associated protein; Pazour et al., 2005), and FAP12 (triacylglycerol lipase), were missing or reduced in the mutant flagella (Fig. 5 B). Therefore, loss of CEP290 affects the flagellar levels of a large number of proteins, including membrane proteins and proteins associated with IFT.

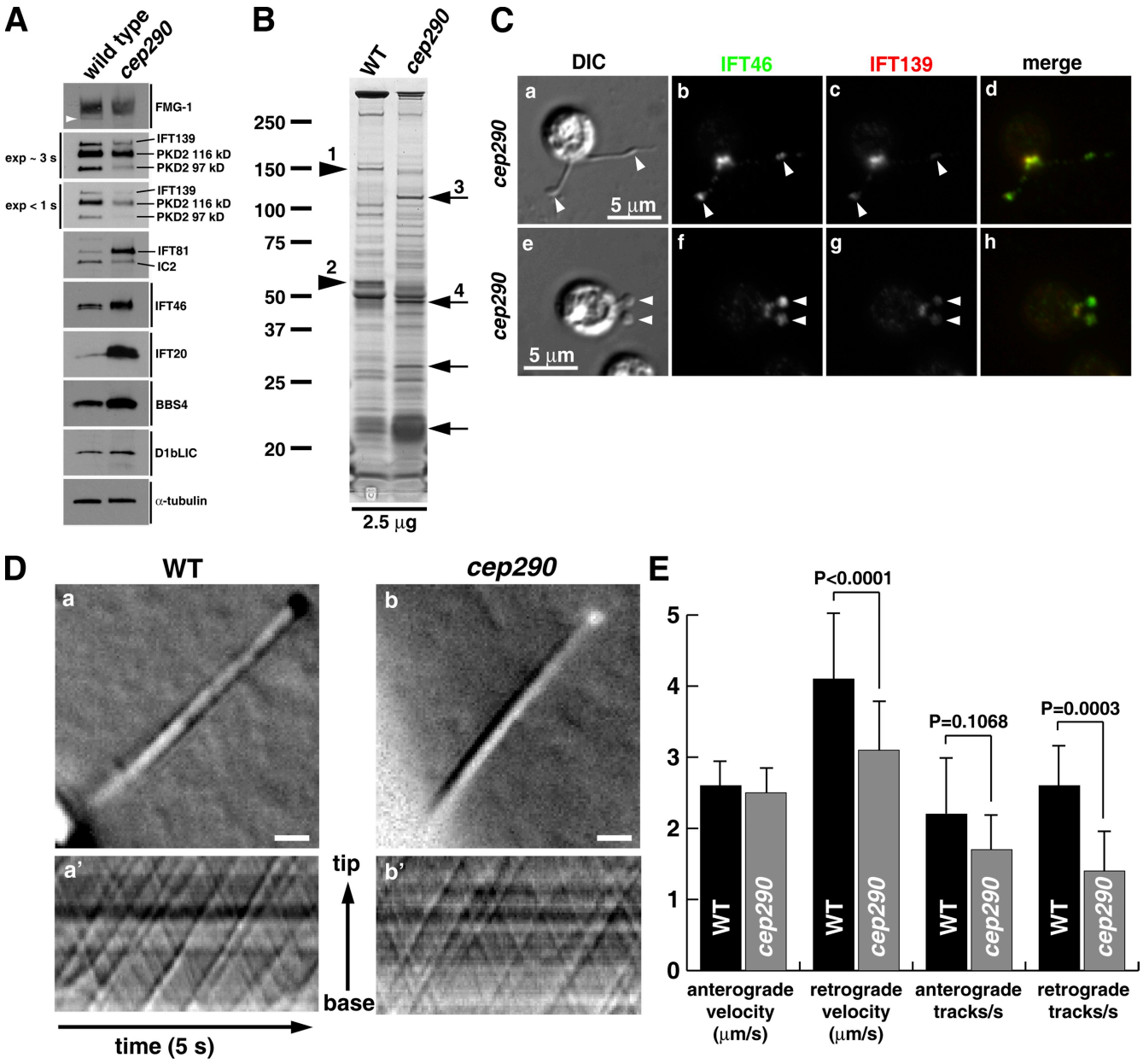


Figure 5. ***cep290* mutant flagella have an abnormal protein composition.** (A) Western blots of isolated flagella show an accumulation of IFT complex B proteins (IFT20, IFT46, and IFT81) and BBS4, and a reduction in the IFT complex A protein IFT139 and polycystin-2 (PKD2). The arrowhead marks an anti–FMG-1-immunoreactive band that is absent in the mutant flagella. (B) Silver-stained gel of isolated wild-type (WT) and mutant (*cep290*) flagella demonstrating that some proteins are abnormally present (arrows) and others are missing or reduced (arrowheads) in the mutant flagella. Proteins identified by mass spectrometry include (1) flagellar adenylate kinase and FAP5, (2) FAP12, (3) EF-3, and (4) EF-1α1. The positions of standard proteins and their molecular masses in kD are indicated. (C) Immunofluorescence indicates that bulges (arrowheads) in the *cep290* mutant flagella contain IFT proteins. (D) DIC imaging and kymographs of IFT in living cells. (D, a and b) Still images of the videos (Videos 5 and 6) used to create the kymographs (a′ and b′). Bars, 1 µm. (E) Velocities and frequencies of IFT in wild-type and *cep290* mutant flagella. Data are represented as mean ± SD (error bars); P-values were determined using a Student's *t* test.

As noted above, some *cep290* mutant flagella have bulges; such bulges in cilia and flagella are usually caused by an accumulation of IFT proteins and defects in retrograde IFT (Pazour et al., 1998, 1999; Piperno et al., 1998; Porter et al., 1999; Iomini et al., 2001, 2009; Hou et al., 2004; Tran et al., 2008). To determine if this is the case in the *cep290* mutant, we localized IFT complex A and B proteins in the mutant cells by immunofluorescence microscopy, and indeed found a concentration of IFT proteins in the flagellar bulges (Fig. 5 C). However, using high-contrast differential interference (DIC) microscopy to observe IFT in live cells, we found that *cep290* mutant cells had normal anterograde IFT, and only a slight decrease in the velocity and frequency of retrograde IFT (Fig. 5, D and E; and Videos 5 and 6). Moreover, our biochemical analysis indicated that the flagellar level of the IFT motor subunit D1bLIC was normal (Fig. 5 A). Therefore, loss of CEP290 has little effect on IFT motility per se.

### CEP290 can incorporate into preassembled wild-type or mutant transition zones

Currently, the only successful approach for treating LCA is somatic gene therapy to replace the defective gene (Bainbridge et al., 2008; Cideciyan et al., 2008; Hauswirth et al., 2008; Maguire et al., 2008). Because the target in the case of CEP290 would be photoreceptor cells, which are not renewed during the life of the organism, this approach would require that CEP290 expressed by a gene therapy vector be incorporated into preassembled ciliary cytoskeletons that lack endogenous CEP290 or have copies of the mutant protein. Although no information is available on whether transition zone components undergo turnover, this can be tested in *C. reinhardtii* using dikaryon rescue. During mating of *C. reinhardtii*, two gametic cells of opposite mating types come into contact and fuse, resulting in a single quadriflagellated, binucleated cell or dikaryon (Harris, 2009). When a wild-type cell is mated to a null mutant, the protein missing in the mutant may be supplied by the wild-type cell, and its ability to be incorporated into the mutant flagellar cytoskeleton then observed. Similarly, when a cell expressing a tagged protein is mated to a wild-type cell, the ability of the tagged protein to displace the endogenous protein in the flagellar cytoskeleton of the untagged partner can be tracked.

We used this technique first to address whether wild-type CEP290 can incorporate into preassembled *cep290* mutant transition zones; i.e., transition zones lacking CEP290. Wild-type and *cep290* mutant gametes were mated, fixed at various time points, and processed for immunofluorescence using antibodies to acetylated tubulin and CEP290. After 20 min, most of the quadriflagellates displayed CEP290 signal on a single pair of transition zones, which must have derived from the wild-type cell; however some of the quadriflagellates at this time point displayed a pair of transition zones with a stronger CEP290 signal and a pair with a weaker signal (presumably the mutant transition zones; Fig. 6 A, a–h). Over the next 40 min, the relative strength of the CEP290 signal on the dimmer pair increased, whereas that on the brighter pair decreased, so that by 60 min all four transition zones had similar signal intensities (Fig. 6 A, i–p). This indicates that wild-type CEP290 can assemble onto previously formed CEP290-deficient transition zones. Moreover, the fact that the brightness of the labeled and unlabeled transition zones equilibrated with time suggested that CEP290 in the transition zone undergoes relatively rapid exchange with CEP290 in the cytoplasm.

Next, to determine if new CEP290 can replace CEP290 previously assembled into wild-type transition zones, we mated wild-type gametes to *cep290::CEP290-HA* gametes, which express only HA-tagged CEP290. The resulting dikaryons were then processed at various times for immunofluorescence microscopy using antibodies to the HA tag and acetylated tubulin (Fig. 6 B). Initially, HA-tagged CEP290 was present only on the two transition zones derived from the HA-tagged parent. After 20 min, CEP290-HA could be observed on all four transition zones, with one pair brighter than the other. Equilibration of the HA signal on all four transition zones occurred by 60 min. Therefore, newly supplied CEP290 can replace CEP290 previously assembled into transition zones. These results confirm that CEP290 is a dynamic component of the transition zone and rapidly equilibrates with cytoplasmic CEP290.

## Discussion

### CEP290 is a component of the microtubule–membrane linkages within the transition zone

The transition zone is a structurally complex and highly conserved structure that lies between the basal body and the flagellar axoneme. The ultrastructure of the *C. reinhardtii* basal body and transition zone has been well characterized (Ringo, 1967; Johnson and Porter, 1968; Cavalier-Smith, 1974; Weiss et al., 1977; Gaffal, 1988; O'Toole et al., 2003; Geimer and Melkonian, 2004). At the distal end of the basal body, the triplet microtubules of the basal body transition into doublets, marking the beginning of the transition zone. Prominent features of the transition zone are structures that bridge the doublet microtubules to the flagellar membrane. In cross sections, these appear as thin Y-shaped connectors (Fig. 3 C); in longitudinal sections, wedge-shaped electron densities are observed to slant proximally and distally from the doublet microtubules to the membrane (Fig. 3 A; Ringo, 1967; Gilula and Satir, 1972; Dentler, 2009a). The central pair microtubules begin at the distal end of the transition zone, marking the beginning of the axoneme.

Although the structure of the transition zone has been described in detail, very little is known regarding the function of this short and unique region of the flagellum (Dutcher, 2009). In addition to its role (along with the basal body) in templating the axoneme, evidence suggests that the transition zone is the site for docking of the IFT particles (Deane et al., 2001). The structure and location of the transition zone make it well poised to act as a flagellar "pore," regulating the import and export of proteins into and out of the flagellum (Rosenbaum and Witman, 2002). The transition zone also has been proposed to be a site for enrichment of $Ca^{2+}$ channels and pumps (Tamm, 1988). Related to this, $Ca^{2+}$-dependent flagellar abscission in *C. reinhardtii* occurs immediately distal to the transition zone (Quarmby, 2009).

Both immunofluorescence microscopy and immuno-EM indicated that CEP290 is located at the transition zone; the immuno-EM showed that the protein is located near the periphery of the transition zone, between the outer doublets and the transition zone membrane. Comparison of the labeling patterns obtained for epitopes at the C terminus versus the central portion of CEP290 indicated that the middle of the protein is closely associated with the wedge-shaped structures seen in longitudinal sections and the Y-shaped connectors seen in cross sections, whereas the C terminus is more dispersed. CEP290 is certainly large enough to account for this distribution of gold particles. In silico analysis of the CEP290 amino acid sequence predicts a high density of coiled-coiled domains throughout the length of the protein. If CEP290 forms a large coiled-coiled structure, it could be as long as ∼380 nm (Fraser and MacRae, 1973) and potentially span the length of the transition zone.

Consistent with the localization of CEP290, the *cep290* mutant cells have striking defects in the structures located between the transition zone doublet microtubules and the flagellar membrane. Specifically, most of the Y connectors seen in cross section were missing, and the wedge-shaped structures seen in longitudinal section were missing or collapsed back onto the doublets. It is

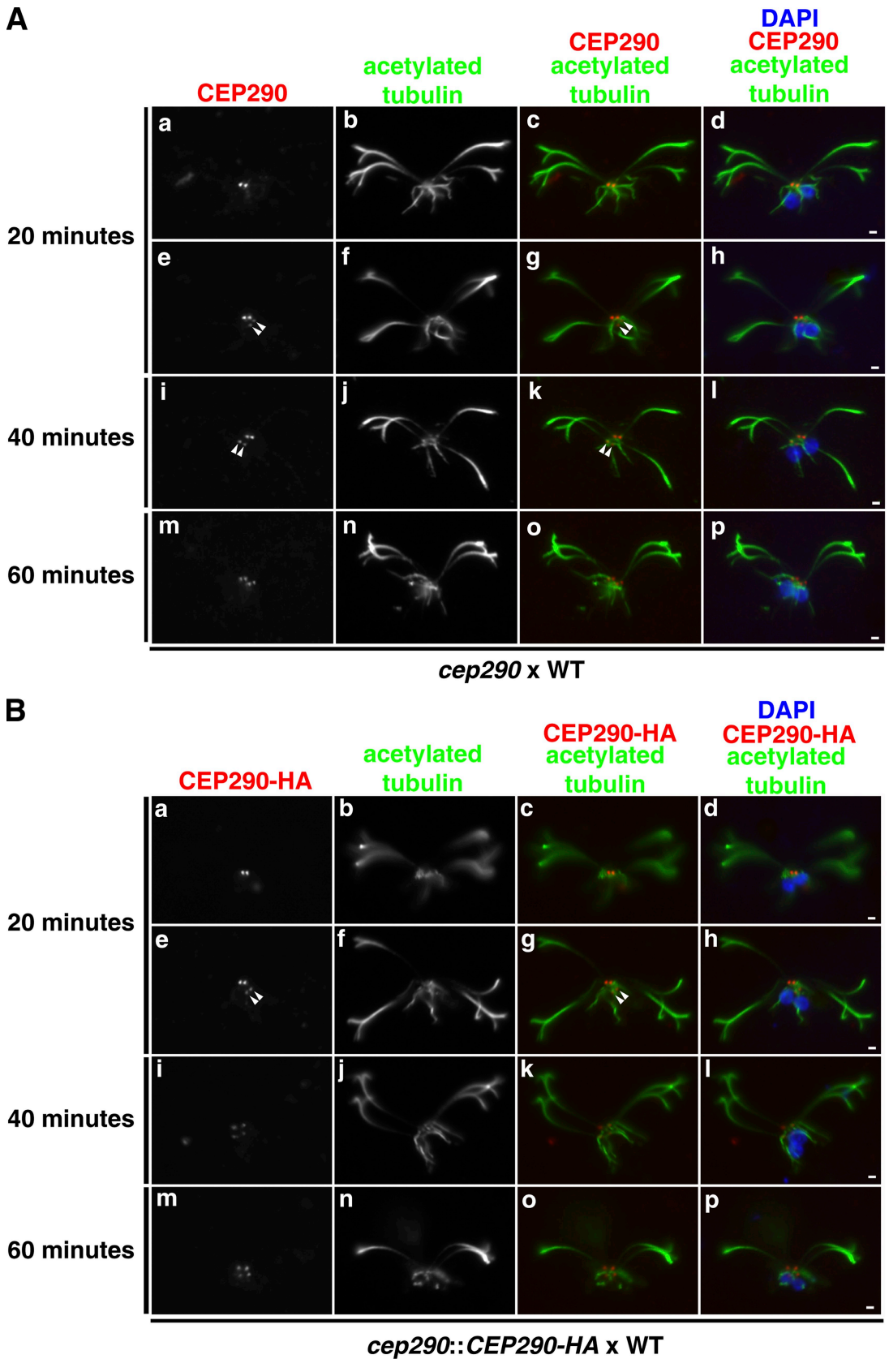


Figure 6. **CEP290 is dynamic and can incorporate into preassembled mutant or wild-type transition zones.** (A) Wild-type gametic cells were mated with *cep290* mutant gametic cells, and the fused, quadriflagellated cells were detergent-extracted, fixed, and processed for immunofluorescence at the indicated time points after the two cell types were mixed for mating. The quadriflagellated cytoskeletons were double labeled with antibodies to CEP290 and acetylated tubulin. Arrowheads mark the dimmer pair of transition zones. (B) Wild-type gametes were mated to *cep290::CEP290-HA* gametes and processed as in A except that CEP290-HA was visualized using anti-HA. Bars, 1 μm.

not yet clear if the Y connector and wedges are one and the same structure viewed from two different angles, but their locations and the fact that both are severely affected in the *cep290* mutant suggest a close relationship. CEP290 is likely to be an essential component of the wedges, because immuno-gold EM showed that the central part of CEP290 is localized to this structure, and the structure is missing when CEP290 is missing. CEP290 antibodies also labeled the Y connectors; however, CEP290 is unlikely to be the only component that comprises them, because Y connectors are seen, albeit rarely, in the null mutant.

Loss of CEP290 and concomitant loss of the transition zone connectors results in loss of attachment of the membrane to the microtubules in the transition zone. Although *C. reinhardtii* mutants with pleiotropic defects in basal bodies and transition zones have been described previously (Goodenough and St. Clair, 1975; Huang et al., 1982; Jarvik and Suhan, 1991; Dutcher and Trabuco, 1998; Piasecki et al., 2008; Piasecki and Silflow, 2009), this is the first study of a mutation that specifically compromises the integrity of the transition zone microtubule–membrane connectors. The results demonstrate that the connectors physically tether the transition zone membrane to the underlying microtubules, a function likely to be important for controlling entry of proteins into the flagellum.

### CEP290 is important for flagellar assembly and protein content

The *cep290* mutant cells are palmelloid, which is a phenotype commonly seen in *C. reinhardtii* mutants with defects in flagellar assembly (Harris, 2009). Indeed, when *cep290* cells are released by digesting the mother cell wall with autolysin, the freshly released cells display very short, stumpy flagella. For reasons not yet understood, the flagella of many *cep290* cells then slowly elongate to various lengths. In mammalian cell culture models, CEP290 siRNA decreases the percentage of cells displaying primary cilia (Graser et al., 2007; Tsang et al., 2008). Collectively, these data indicate a conserved requirement for CEP290 in ciliogenesis.

SDS-PAGE revealed numerous differences in the flagellar proteins of wild type versus the *cep290* mutant; some of these were identified by mass spectrometry. Notably, *cep290* flagella have reduced amounts of flagellar adenylate kinase; of FAP12, which is predicted to be a triacylglycerol lipase; and of FAP5, which is a conserved flagellar-associated protein of unknown function (Pazour et al., 2005). Loss of flagellar adenylate kinase could affect ATP production in the flagellum, whereas loss of triacylglycerol lipase could affect flagellar membrane lipid composition. Thus, either of these deficiencies could affect flagellar assembly. EF-3 and EF-1α were elevated in *cep290* flagella; the functions of these proteins in flagella are unknown.

The flagella of *cep290* mutant cells occasionally have bulges filled with a finely divided material that includes IFT proteins, and Western blot analysis of isolated flagella revealed that the mutant flagella accumulate IFT complex B proteins and have decreased levels of the IFT complex A component IFT139. When *cep290* cells were compared with wild-type cells, there was no significant difference in anterograde IFT, but retrograde IFT was slightly reduced both in velocity and frequency. The decrease in retrograde IFT velocity may be related to the decrease in IFT complex A and/or the accumulation of complex B in the mutant flagella, as similar decreases in retrograde IFT velocities have been observed in complex A mutants, which also have increased complex B and decreased complex A in their flagella (Piperno et al., 1998; Iomini et al., 2001, 2009). In any case, it seems unlikely that a defect in IFT motility per se is the cause of the abnormal balance of IFT complexes A and B in the *cep290* flagella. It should be noted that other *C. reinhardtii* mutants accumulate IFT proteins in bulges at the flagellar tip yet display normal velocities and frequencies of IFT (Tam et al., 2003; Dentler, 2005).

We propose that the abnormal balance of IFT particles and the abnormal protein composition of *cep290* mutant flagella result from loss of the microtubule–membrane connectors, with concomitant defects in the remodeling, cargo loading/unloading, or "quality control" of IFT particles as they pass through the transition zone. CEP290 and the membrane connectors within the transition zone could provide a platform for IFT particles as they are loaded and unloaded at the base of the flagellum, a checkpoint that admits only proteins with flagellar targeting sequences, or a "gate" through which only properly assembled IFT particles can pass. Loss of the gate may allow an excess of IFT complex B proteins to enter the flagellum, where they accumulate without the proper complement of IFT complex A, which may be necessary to couple them to the retrograde IFT motor for export from the flagellum (Hao and Scholey, 2009). Alternatively, the membrane connectors and/or CEP290 might be required for the efficient entry of IFT complex A into the flagellum; defects in complex A trafficking could also result in the accumulation of IFT complex B, as is seen in *C. reinhardtii* strains with mutations in IFT complex A components (Piperno et al., 1998; Iomini et al., 2001, 2009). Because IFT is necessary for flagellar assembly and maintenance, such defects could in turn lead to the many other abnormalities in flagellar protein content that we observed. Previous studies reported mislocalization of some ciliary components in mice harboring a hypomorphic mutation in *Cep290* (Chang et al., 2006; McEwen et al., 2007). Here, we demonstrate that loss of CEP290 affects the normal levels of IFT particles in the flagellum, which could provide mechanistic insight into why defects in CEP290 affect ciliary assembly and the localization of other ciliary proteins.

### Loss of CEP290 results in abnormal flagellar levels of ciliary disease proteins

Among the abnormalities in *cep290* mutant flagella is a decreased level of polycystin-2, an important observation given the prevalence of cystic kidneys in patients with *CEP290* mutations. Polycystin-2 is a six-pass transmembrane protein that localizes to cilia and forms a cation-permeable channel; mutations in the human gene (*PKD2*) are the cause of autosomal dominant polycystic kidney disease type 2 (OMIM no. 613095). Our results demonstrate that CEP290 is required for normal levels of polycystin-2 in flagella, and suggest that cystic kidney disease in patients with *CEP290* mutations could result from defects in the ciliary levels of polycystin-2.

Many of the disease symptoms caused by *CEP290* mutations are also present in patients with Bardet-Biedl syndrome (BBS; OMIM no. 209900), and a homozygous mutation in

*CEP290* (E1903X) was found in a BBS patient that also carried a complex heterozygous mutation in *MKS3* (Leitch et al., 2008). Flagella of the *cep290* mutant have increased levels of BBS4, which is a component of the BBSome (Nachury et al., 2007) and is trafficked in the flagellum by a subset of IFT particles (Lechtreck et al., 2009). This raises the possibility that the amount of BBSomes in the flagellum is determined by the same factors that control the amount of complex B, which is also increased in *cep290* flagella. In any case, the BBSome is required for the removal of specific signaling proteins (e.g., phospholipase D) from flagella (Lechtreck et al., 2009), and the phenotypic overlap between BBS and CEP290-associated ciliopathies could be explained, at least in part, by the accumulation of BBS4 in *cep290* mutant cilia. It is unknown if CEP290 interacts directly with the BBSome, but both CEP290 and BBS4 interact with the pericentriolar protein PCM-1 (Kim et al., 2004; Kim et al., 2008), and CEP290 depletion by siRNA shifted the sedimentation profile of BBS4 in sucrose gradients (Kim et al., 2008).

Finally, given our finding that CEP290 is a component of the transition zone, it is relevant that the connecting cilia of mammalian photoreceptor cells are thought to be greatly elongated transition zones (Besharse and Horst, 1990) and contain microtubule–membrane Y connectors analogous to those seen in the *C. reinhardtii* transition zone. Mutations in human *CEP290* almost always are associated with blindness, regardless of whether or not other organs are affected, so CEP290 may be especially important in the function of the connecting cilium, through which huge amounts of precisely sorted IFT-dependent cargo must pass each day to maintain the photoreceptor outer segment.

### CEP290 is dynamically associated with the transition zone

LCA caused by mutations in *RPE65* has been treated by gene therapy, with some individuals experiencing improvement in visual acuity (Bainbridge et al., 2008; Cideciyan et al., 2008; Hauswirth et al., 2008; Maguire et al., 2008). It has been estimated that ∼20% of LCA cases are caused by mutations in *CEP290* (den Hollander et al., 2006), making *CEP290* an important target for gene therapy in these patients. We demonstrated that CEP290 is dynamic and can incorporate into preassembled CEP290-deficient and wild-type transition zones, a property that will be essential for successful *CEP290* gene therapy in the retina.

Our results indicate that CEP290 shuttles between the transition zone and the cytoplasm. In mammalian cells, CEP290 redistributes to the cytosol during mitosis (Sayer et al., 2006), a time in the cell cycle when cilia are not present. In addition, CEP290 contains a putative nuclear localization signal (Chang et al., 2006; Sayer et al., 2006) that is conserved in *C. reinhardtii*, CEP290 has been detected in the nucleus (Guo et al., 2004; Sayer et al., 2006), and CEP290 has been shown to activate the transcription factor ATF4 in a luciferase reporter assay (Sayer et al., 2006). Thus, CEP290 may also be involved in signal transduction. The location of CEP290 at the transition zone and its dynamic properties would make it ideally suited for monitoring flagellar status and relaying information about the flagellum back to the cell body or nucleus.

In summary, our results show that CEP290 is a transition zone protein localized to and required for the assembly of the unique microtubule–membrane connectors in this region. Loss of CEP290 and these structures results in an imbalance of IFT complexes in the flagellum, and leads to numerous other abnormalities in the composition of flagella, including abnormal levels of flagellar membrane proteins and proteins associated with ciliopathies. Similar changes in ciliary protein composition are almost certain to be the underlying cause of the human pathologies resulting from *CEP290* mutation.

## Materials and methods

#### Strains and cell culture

Strains were grown in liquid M medium I (Sager and Granick, 1953), with 2.2 mM $KH_2PO_4$ and 1.71 mM $K_2HPO_4$, aeration by 5% $CO_2$, and a light/dark cycle of 14/10 h (Witman, 1986). For some experiments, cells were cultured without aeration or treated with autolysin in order to induce flagellation. The following *C. reinhardtii* strains were used: 137c (CC-125; *nit1, nit2, mt+*), g1 (*nit1, agg1, mt+*), CC-124 (*nit1, nit2, agg1, mt−*), Y168 (*nit1::NIT1, agg1, cep290, mt+*), F1P4 (*nit1::NIT1, agg1, cep290, mt−*), *cep290* (*nit1::NIT1, agg1, cep290, mt+*), *cep290::CEP290* (*nit1::NIT1, agg1, cep290::CEP290, mt−*), and *cep290::CEP290-HA* (*nit1::NIT1, agg1, cep290::CEP290-HA, mt+*).

#### Antibodies

A synthetic peptide consisting of the last 14 amino acids of *C. reinhardtii* CEP290 with cysteine added to the N terminus for conjugation to KLH (C-ADGAGPSGQRRGGR) was used to generate rabbit polyclonal antibodies (GenScript). The resulting antiserum was affinity purified on an agarose support (Thermo Fisher Scientific) according to the manufacturer's instructions. Additional antibodies used in this study were: rat high-affinity anti-HA (Roche), anti-acetylated tubulin (Sigma-Aldrich), anti–α-tubulin (Sigma-Aldrich), anti-polyglutamylated tubulin (Wolff et al., 1992), anti–β-$F_1$-ATPase (Agrisera), anti-BBS4 (Lechtreck et al., 2009), anti-IC2 (King et al., 1985), anti-FMG1 (provided by R. Bloodgood, University of Virginia, Charlottesville, VA; Bloodgood et al., 1986), anti-PKD2 "loop" (provided by K. Huang, Yale University, New Haven, CT; Huang et al., 2007), anti-D1bLIC (Hou et al., 2004), anti-IFT20 (Hou et al., 2007), anti-IFT46 (provided by H. Qin, Texas A&M University, College Station, TX; Hou et al., 2007), and anti-IFT81 and anti-IFT139 (provided by D. Cole, University of Idaho, Moscow, ID; Cole et al., 1998).

#### RT-PCR screen and backcrossing

A library of insertional mutants was screened by real-time PCR using the QuantiTect SYBR Green PCR kit (QIAGEN) and primer pairs (see Table S1) specific for the 5′ and 3′ ends of *C. reinhardtii CEP290*. Additional primer pairs were used to map the deletion in strain Y168. Y168 was backcrossed to wild type (CC-124) and the Y168 mutant phenotype cosegregated with the deletion. A mutant progeny (F1P4) from this cross was then backcrossed to the Y168 parent strain (g1 [Pazour et al., 1995], used as the wild-type control strain for this study) and the mutant phenotype again cosegregated with the deletion. A mutant progeny from the second backcross, strain *cep290*, was used for the remainder of the study.

#### Cloning the *CEP290* gene and rescue of the *cep290* mutant

First, a cassette conferring phleomycin resistance (Stevens et al., 1996; Lumbreras et al., 1998) was cloned into the HindIII site in pNEB193 (New England Biolabs, Inc.) to make pBC1. Second, a bacterial artificial chromosome (BAC) containing *C. reinhardtii CEP290* (BAC 29K10, Clemson University Genomics Institute) was digested with AscI and StuI to obtain a 9.3-kb fragment that was cloned into pBC1 cut with AscI and PmeI, yielding pBC2. Third, the BAC was digested with ApoI and AscI, and a 6-kb fragment was purified and cloned into pBC2 also cut with ApoI and AscI, yielding pBC3. To introduce a triple HA tag, p3×HA (Silflow et al., 2001) was digested with SmaI and NaeI, and the resulting fragment containing the 3×HA sequence was cloned into pBC3 by partially digesting pBC3 with ScaI, yielding pBC4. All constructs were verified by sequencing. 5 µg of pBC3 or pBC4 plasmid linearized with SspI were used to transform the F1P4 CEP290 mutant strain or the *cep290* strain, respectively, using glass bead agitation (Kindle, 1990). Rescued transformants were identified visually by screening for wild-type

motility, and the presence of the rescuing construct was confirmed by PCR and Western blotting.

**Live cell imaging and videos**

Cells were cultured as described above, placed into an 8-well slide, and sealed with Vaseline and a coverslip. The cells were visualized by dark-field phase contrast using a microscope (Axioskop II plus; Carl Zeiss, Inc.) equipped with a 10× Plan-Neofluar objective lens. Images were captured at 30 frames/second with a UNIQ UP-610 digital charge-coupled device camera, and image sequences were output as AVI files and processed using ImageJ software, then converted into MOV files using QuickTime Pro (Apple). To document motility (Fig. 1 B), the WalkingAverage function in ImageJ was used to average 30 frames. For DIC imaging of IFT (summarized in Dentler et al., 2009b), live cells were immobilized in 1% agarose, sealed in an eight-well slide as described above, and observed using an inverted microscope (Ti U; Nikon) equipped with a 60× 1.49 NA objective lens, a 1.4 NA oil condenser, a 1.5× relay lens, and DIC optics. Illumination was provided by a Lumen 200 (Prior Scientific) light source, and light was filtered through UV, green band pass, and heat-absorbing filters. Images were captured at 24 frames per second with a Clara Interline camera (Andor) and NIS-Elements software (Nikon). Image sequences were cropped, image brightness and contrast was adjusted in ImageJ, and the resulting image stacks were exported as AVI files using ImageJ, then converted into MOV files using QuickTime Pro. Kymographs were generated in ImageJ by drawing a line that included the entire width of the flagellum (width 11) and the MultipleKymograph ImageJ plugin with a line width of 1. IFT velocities and frequencies were calculated by measuring the slope and number of the particle tracks in the kymographs, respectively.

**Immunofluorescence microscopy**

Cells were cultured as described above and harvested by centrifugation. In some experiments, cells were treated with autolysin for 1–2 h before processing for immunofluorescence to induce the growth of flagella. For immunofluorescence of whole cells, cells were allowed to adhere for 5 min to polyethylenimine-coated coverslips, excess cells were wicked off, and the coverslips were submerged in −20°C methanol for 20 min. The slips were then air-dried, rehydrated, and blocked for 30 min at RT with blocking solution (6% fish skin gelatin, 1% BSA, and 0.05% Tween-20 in PBS, pH 7.0), incubated with primary antibodies (either 30–60 min at RT or 4°C overnight), washed 3× with blocking solution, incubated with secondary antibodies (Alexa Fluor–conjugated IgG; Invitrogen) for 30 min at RT, washed 3× with PBS, then mounted with ProLong Antifade Gold (Invitrogen). For immunofluorescence of isolated cytoskeletons, cells were harvested by centrifugation, resuspended in autolysin for 1–2 h, washed once with HMDEK (30 mM Hepes, pH 7.4, 5 mM $MgSO_4$, 1 mM DTT, 0.5 mM EGTA, and 25 mM KCl), resuspended in HMDEK, and chilled on ice. Then, an equal volume of ice-cold HMDEK + 2% NP-40 Alternative (EMD) + 2× Complete Protease Inhibitor (Roche) was added. The cells were lysed on ice for 15 min then added to an equal volume of RT HMDEK + 4% paraformaldehyde, and the detergent-extracted cytoskeletons were adhered onto poly-L-lysine–coated coverslips for 15 min. The slips were rinsed twice with PBS, then air-dried. The slips were then blocked, incubated with antibody, and mounted as described above. Samples were imaged using a microscope (Axioskop II plus) with a 100× Plan-Apochromat 1.4 NA objective equipped with a DIC prism. Images were captured with a digital charge-coupled device camera (MrM) and Axiovision software (both from Carl Zeiss, Inc.). When applicable, Photoshop (Adobe) was used to make equal brightness and/or contrast adjustments for samples under comparison.

**EM**

For ultrastructural analysis, cells were harvested by centrifugation, gently resuspended in conditioned medium, and then fixed by addition of an equal volume of 2% glutaraldehyde in conditioned medium. After 15 min at RT, the cells were pelleted, the primary fixative was removed, and the cells were gently resuspended in secondary fixative (1% glutaraldehyde and 100 mM sodium cacodylate, pH 7.2) and incubated for 2 h at RT. The cells were then pelleted and washed three times for 15 min each with 100 mM sodium cacodylate, pH 7.2. After the final wash, 50 µl of cell pellet was removed and added to a microcentrifuge tube containing 50 µl of 2% agarose dissolved in 100 mM sodium cacodylate, pH 7.2. The cell/agarose suspension was solidified on ice, and the solidified cell/agarose block was removed by cutting off the bottom of the microcentrifuge tube. The cell/agarose block was then cut into ∼1 $mm^2$ pieces, post-fixed for 1 h on ice with 1% $OsO_4$ in 50 mM sodium cacodylate, washed three times with ice-cold water, and stained overnight at 4°C in freshly prepared 1% uranyl acetate in water. The samples were then dehydrated, embedded in epon, and thin-sectioned. Sections were stained with lead citrate and imaged on an electron microscope (CM10; Philips). Images were acquired using a digital camera (Gatan). For image averages, 30 wild-type or mutant cross-sections were aligned and superimposed over each other with 10% transparency using Photoshop (Adobe). For analysis of detergent-resistant membranes (Kamiya and Witman, 1984), cytoskeletons were prepared as described above (Immunofluorescence microscopy) then fixed and processed for EM as described.

For immuno-EM, cytoskeletons were prepared as above (Immunofluorescence microscopy) and fixed with 3% paraformaldehyde in MT buffer (30 mM Hepes, 5 mM EGTA, 15 mM KCl, and 5 mM MgSO4, pH 7.2) on ice for 20 min. After blocking in 2% BSA with 0.1% cold fish skin gelatin and 0.05% Tween-20 in PBS for 1 h, the samples were labeled with primary antibody (1:25 rabbit anti-CEP290 and 1:50 rat anti-HA monoclonal 3F10) and gold-conjugated secondary antibody (1:20 goat anti–rabbit 12-nm gold conjugant and 1:20 goat anti–rat 6-nm gold conjugant) for 90 min each, then postfixed with 2.5% glutaraldehyde with 0.1% tannic acid for 1 h, followed by 1% $OsO_4$ at 4°C for 1 h. Sections were stained with 2% uranyl acetate in methanol for 10 min.

**Flagella isolation, SDS-PAGE, Western blotting, and mass spectrometry**

To induce *cep290* cells to hatch and assemble flagella, cells were cultured in minimal medium in the absence of aeration. For comparisons, control wild-type cells were cultured under identical conditions. Flagella were harvested using dibucaine (Witman et al., 1972; Witman, 1986) and resuspended in HMDEK supplemented with Complete Protease Inhibitor Cocktail (Roche). Protein concentration of isolated flagella was determined using the RC-DC Protein Assay (BioRad Laboratories). Equal amounts of wild-type and mutant flagellar protein were analyzed by SDS-PAGE and silver staining (BioRad Laboratories) or Western blotting. Silver-stained bands of interest were excised and identified by mass spectrometry as described previously (Lechtreck et al., 2009). For Western blots of whole-cell lysates, mid-log phase cells were harvested by centrifugation, resuspended in 5× denaturing sample buffer (50 mM Tris, pH 8.0, 160 mM DTT, 5 mM EDTA, pH 8.0, 50% sucrose, and 5% SDS), heated at 75°C for 5 min, then passed through a 26-gauge needle three times.

**Gamete generation and mating, crude autolysin production, and dikaryon formation**

To generate gametes, 137c (*mt+*) and CC124 (*mt−*) cells were plated onto TAP medium plates with 1.5% agar (Harris, 2009), grown for 5–7 d in cycled light, then placed in dim cycled light for 2–4 wk. The cells were then scraped into 10 ml of nitrogen-free medium (M-N) and agitated on an orbital shaker overnight with continuous light in a 125-ml flask. The next morning, the cells were gently collected by centrifugation, resuspended in 10 ml of M-N diluted 1:5 with water + 10 mM Hepes, pH 7.4, and subjected to ∼4 h of orbital rotation under constant light. For production of crude autolysin, gametes of the two cell types were mixed for 5 min and centrifuged, and the supernatant was filtered through a 0.8/0.2-µm syringe filter. Autolysin was either used immediately or flash-frozen with liquid nitrogen and stored at −80°C. To mate cells for backcrossing, gametic cells were treated for 1–2 h with autolysin to hatch *cep290* gametes, and then mixed for 1–2 h. The zygotes were then plated onto M medium plates with 4% agar and cultured for 24 h under constant light. Progeny from tetrads were isolated as described previously (Pazour et al., 1999; Hou et al., 2004), and real-time PCR was used to identify the progeny harboring the deletion in *CEP290*. For experiments involving dikaryons, gametes of opposite mating types were mixed for various time points. The cells were then detergent-extracted and processed for immunofluorescence as described above (Immunofluorescence microscopy).

**Flagellar regeneration**

Mid-log phase cells were concentrated twofold and the pH was quickly lowered to 4.5 by the addition of 0.5 N acetic acid. After 45 s, the pH was neutralized to 7.0 by the addition of 0.5 N KOH. The cells were then fixed and processed for immunofluorescence microscopy at various time points.

**Online supplemental material**

Fig. S1 shows that CEP290 remains at the transition zone after flagellar abscission and during flagellar regeneration. Fig. S2 shows that CEP290 is not present in isolated flagella. Fig. S3 shows a representative selection of EMs that were used to generate Fig. 4 A. Fig. S4 shows a representative selection of EMs used to generate Fig. 4 (B and C). Videos 1–4 show the motility of wild-type, the *cep290* mutant, the *cep290* mutant following rescue with untagged CEP290, and the *cep290* mutant following rescue with HA-tagged CEP290, respectively. Videos 5 and 6 show the

movement of IFT particles in wild-type and *cep290* mutant flagella, respectively. Online supplemental material is available at http://www.jcb.org/cgi/content/full/jcb.201006105/DC1.

We thank Drs. R. Bloodgood (University of Virginia, Charlottesville, VA), D. Cole (University of Idaho, Moscow, ID), B. Eddé (Centre National de la Recherche Scientifique, Montpellier, France) K. Huang (Yale University, New Haven, CT), and H. Qin (Texas A&M University, College Station, TX) for kindly providing antibodies used in this study. We are grateful to D. M. Sanderson (University of Massachusetts Medical School) for the loan of microscopy equipment.

This research was supported by National Institutes of Health grants (GM030626 to G.B. Witman, GM087848 to B. Craige, and GM014642 to J.L. Rosenbaum), the Grousbeck Family Foundation (to G.B. Witman and J.L. Rosenbaum), and the Robert W. Booth Endowment (to G.B. Witman). G.B. Witman is a member of the University of Massachusetts Medical School Diabetes and Endocrinology Research Center (DERC; DK32520), and core resources used in this research were supported by a DERC grant (DK32520).

Submitted: 16 June 2010
Accepted: 11 August 2010

## References

Andersen, J.S., C.J. Wilkinson, T. Mayor, P. Mortensen, E.A. Nigg, and M. Mann. 2003. Proteomic characterization of the human centrosome by protein correlation profiling. *Nature.* 426:570–574. doi:10.1038/nature02166

Baala, L., S. Audollent, J. Martinovic, C. Ozilou, M.C. Babron, S. Sivanandamoorthy, S. Saunier, R. Salomon, M. Gonzales, E. Rattenberry, et al. 2007. Pleiotropic effects of *CEP290 (NPHP6)* mutations extend to Meckel syndrome. *Am. J. Hum. Genet.* 81:170–179. doi:10.1086/519494

Badano, J.L., N. Mitsuma, P.L. Beales, and N. Katsanis. 2006. The ciliopathies: an emerging class of human genetic disorders. *Annu. Rev. Genomics Hum. Genet.* 7:125–148. doi:10.1146/annurev.genom.7.080505.115610

Bainbridge, J.W., A.J. Smith, S.S. Barker, S. Robbie, R. Henderson, K. Balaggan, A. Viswanathan, G.E. Holder, A. Stockman, N. Tyler, et al. 2008. Effect of gene therapy on visual function in Leber's congenital amaurosis. *N. Engl. J. Med.* 358:2231–2239. doi:10.1056/NEJMoa0802268

Besharse, J.C., and C.J. Horst. 1990. The photoreceptor connecting cilium: a model for the transition zone. *In* Ciliary and Flagellar Membranes. R.A. Bloodgood, editor. Plenum Press, New York. 389–417.

Bloodgood, R.A., M.P. Woodward, and N.L. Salomonsky. 1986. Redistribution and shedding of flagellar membrane glycoproteins visualized using an anti-carbohydrate monoclonal antibody and concanavalin A. *J. Cell Biol.* 102:1797–1812. doi:10.1083/jcb.102.5.1797

Brancati, F., G. Barrano, J.L. Silhavy, S.E. Marsh, L. Travaglini, S.L. Bielas, M. Amorini, D. Zablocka, H. Kayserili, L. Al-Gazali, et al. 2007. *CEP290* mutations are frequently identified in the oculo-renal form of Joubert syndrome-related disorders. *Am. J. Hum. Genet.* 81:104–113. doi:10.1086/519026

Cavalier-Smith, T. 1974. Basal body and flagellar development during the vegetative cell cycle and the sexual cycle of *Chlamydomonas reinhardii*. *J. Cell Sci.* 16:529–556.

Chang, B., H. Khanna, N. Hawes, D. Jimeno, S. He, C. Lillo, S.K. Parapuram, H. Cheng, A. Scott, R.E. Hurd, et al. 2006. In-frame deletion in a novel centrosomal/ciliary protein CEP290/NPHP6 perturbs its interaction with RPGR and results in early-onset retinal degeneration in the *rd16* mouse. *Hum. Mol. Genet.* 15:1847–1857. doi:10.1093/hmg/ddl107

Cideciyan, A.V., T.S. Aleman, S.L. Boye, S.B. Schwartz, S. Kaushal, A.J. Roman, J.J. Pang, A. Sumaroka, E.A. Windsor, J.M. Wilson, et al. 2008. Human gene therapy for RPE65 isomerase deficiency activates the retinoid cycle of vision but with slow rod kinetics. *Proc. Natl. Acad. Sci. USA.* 105:15112–15117. doi:10.1073/pnas.0807027105

Cole, D.G., D.R. Diener, A.L. Himelblau, P.L. Beech, J.C. Fuster, and J.L. Rosenbaum. 1998. *Chlamydomonas* kinesin-II-dependent intraflagellar transport (IFT): IFT particles contain proteins required for ciliary assembly in *Caenorhabditis elegans* sensory neurons. *J. Cell Biol.* 141:993–1008. doi:10.1083/jcb.141.4.993

Deane, J.A., D.G. Cole, E.S. Seeley, D.R. Diener, and J.L. Rosenbaum. 2001. Localization of intraflagellar transport protein IFT52 identifies basal body transitional fibers as the docking site for IFT particles. *Curr. Biol.* 11:1586–1590. doi:10.1016/S0960-9822(01)00484-5

den Hollander, A.I., R.K. Koenekoop, S. Yzer, I. Lopez, M.L. Arends, K.E. Voesenek, M.N. Zonneveld, T.M. Strom, T. Meitinger, H.G. Brunner, et al. 2006. Mutations in the *CEP290* (*NPHP6*) gene are a frequent cause of Leber congenital amaurosis. *Am. J. Hum. Genet.* 79:556–561. doi:10.1086/507318

Dentler, W. 2005. Intraflagellar transport (IFT) during assembly and disassembly of *Chlamydomonas* flagella. *J. Cell Biol.* 170:649–659. doi:10.1083/jcb.200412021

Dentler, W. 2009a. Microtubule-membrane interactions in *Chlamydomonas* flagella. *In* The *Chlamydomonas* Sourcebook. Volume 3. G.B. Witman, editor. Academic Press/Elsevier, New York. 283–307.

Dentler, W., K. VanderWall, and M.E. Porter. 2009b. Recording and analyzing IFT in *Chlamydomonas* flagella. *In* Cilia: Model Organisms and Intraflagellar Transport. S.M. King, and G.J. Pazour, editors. Academic Press, New York. 145–155.

Dutcher, S.K. 2009. Basal bodies and associated structures. *In* The *Chlamydomonas* Sourcebook. Volume 3. G.B. Witman, editor. Academic Press/Elsevier, New York. 15–42.

Dutcher, S.K., and E.C. Trabuco. 1998. The *UNI3* gene is required for assembly of basal bodies of *Chlamydomonas* and encodes delta-tubulin, a new member of the tubulin superfamily. *Mol. Biol. Cell.* 9:1293–1308.

Fliegauf, M., T. Benzing, and H. Omran. 2007. When cilia go bad: cilia defects and ciliopathies. *Nat. Rev. Mol. Cell Biol.* 8:880–893. doi:10.1038/nrm2278

Frank, V., A.I. den Hollander, N.O. Brüchle, M.N. Zonneveld, G. Nürnberg, C. Becker, G. Du Bois, H. Kendziorra, S. Roosing, J. Senderek, et al. 2008. Mutations of the *CEP290* gene encoding a centrosomal protein cause Meckel-Gruber syndrome. *Hum. Mutat.* 29:45–52. doi:10.1002/humu.20614

Fraser, R.D.B., and T.P. MacRae. 1973. Conformation in Fibrous Proteins and Related Synthetic Polypeptides. Academic Press, New York. 628 pp.

Gaffal, K.P. 1988. The basal body-root complex of *Chlamydomonas reinhardtii* during mitosis. *Protoplasma.* 143:118–129. doi:10.1007/BF01291156

Geimer, S., and M. Melkonian. 2004. The ultrastructure of the *Chlamydomonas reinhardtii* basal apparatus: identification of an early marker of radial asymmetry inherent in the basal body. *J. Cell Sci.* 117:2663–2674. doi:10.1242/jcs.01120

Gilula, N.B., and P. Satir. 1972. The ciliary necklace. A ciliary membrane specialization. *J. Cell Biol.* 53:494–509. doi:10.1083/jcb.53.2.494

Goodenough, U.W., and H.S. St. Clair. 1975. *BALD-2*: a mutation affecting the formation of doublet and triplet sets of microtubules in *Chlamydomonas reinhardtii*. *J. Cell Biol.* 66:480–491. doi:10.1083/jcb.66.3.480

Graser, S., Y.D. Stierhof, S.B. Lavoie, O.S. Gassner, S. Lamla, M. Le Clech, and E.A. Nigg. 2007. Cep164, a novel centriole appendage protein required for primary cilium formation. *J. Cell Biol.* 179:321–330. doi:10.1083/jcb.200707181

Guo, J., G. Jin, L. Meng, H. Ma, D. Nie, J. Wu, L. Yuan, and C. Shou. 2004. Subcellullar localization of tumor-associated antigen 3H11Ag. *Biochem. Biophys. Res. Commun.* 324:922–930. doi:10.1016/j.bbrc.2004.09.133

Hao, L., and J.M. Scholey. 2009. Intraflagellar transport at a glance. *J. Cell Sci.* 122:889–892. doi:10.1242/jcs.023861

Harris, E.H. 2009. The *Chlamydomonas* Sourcebook. Volume 1. Elsevier/Academic Press, Amsterdam. 444 pp.

Hauswirth, W.W., T.S. Aleman, S. Kaushal, A.V. Cideciyan, S.B. Schwartz, L. Wang, T.J. Conlon, S.L. Boye, T.R. Flotte, B.J. Byrne, and S.G. Jacobson. 2008. Treatment of leber congenital amaurosis due to *RPE65* mutations by ocular subretinal injection of adeno-associated virus gene vector: short-term results of a phase I trial. *Hum. Gene Ther.* 19:979–990. doi:10.1089/hum.2008.107

Helou, J., E.A. Otto, M. Attanasio, S.J. Allen, M.A. Parisi, I. Glass, B. Utsch, S. Hashmi, E. Fazzi, H. Omran, et al. 2007. Mutation analysis of *NPHP6/CEP290* in patients with Joubert syndrome and Senior-Løken syndrome. *J. Med. Genet.* 44:657–663. doi:10.1136/jmg.2007.052027

Hou, Y., G.J. Pazour, and G.B. Witman. 2004. A dynein light intermediate chain, D1bLIC, is required for retrograde intraflagellar transport. *Mol. Biol. Cell.* 15:4382–4394. doi:10.1091/mbc.E04-05-0377

Hou, Y., H. Qin, J.A. Follit, G.J. Pazour, J.L. Rosenbaum, and G.B. Witman. 2007. Functional analysis of an individual IFT protein: IFT46 is required for transport of outer dynein arms into flagella. *J. Cell Biol.* 176:653–665. doi:10.1083/jcb.200608041

Huang, B., Z. Ramanis, S.K. Dutcher, and D.J. Luck. 1982. Uniflagellar mutants of *Chlamydomonas*: evidence for the role of basal bodies in transmission of positional information. *Cell.* 29:745–753. doi:10.1016/0092-8674(82)90436-6

Huang, K., D.R. Diener, A. Mitchell, G.J. Pazour, G.B. Witman, and J.L. Rosenbaum. 2007. Function and dynamics of PKD2 in *Chlamydomonas reinhardtii* flagella. *J. Cell Biol.* 179:501–514. doi:10.1083/jcb.200704069

Iomini, C., V. Babaev-Khaimov, M. Sassaroli, and G. Piperno. 2001. Protein particles in *Chlamydomonas* flagella undergo a transport cycle consisting of four phases. *J. Cell Biol.* 153:13–24. doi:10.1083/jcb.153.1.13

Iomini, C., L. Li, J.M. Esparza, and S.K. Dutcher. 2009. Retrograde intraflagellar transport mutants identify complex A proteins with multiple genetic

interactions in *Chlamydomonas reinhardtii*. *Genetics.* 183:885–896. doi:10.1534/genetics.109.101915

Jarvik, J.W., and J.P. Suhan. 1991. The role of the flagellar transition region: inferences from the analysis of a *Chlamydomonas* mutant with defective transition region structures. *J. Cell Sci.* 99:731–740.

Johnson, U.G., and K.R. Porter. 1968. Fine structure of cell division in *Chlamydomonas reinhardi*. Basal bodies and microtubules. *J. Cell Biol.* 38:403–425. doi:10.1083/jcb.38.2.403

Kamiya, R., and G.B. Witman. 1984. Submicromolar levels of calcium control the balance of beating between the two flagella in demembranated models of *Chlamydomonas*. *J. Cell Biol.* 98:97–107. doi:10.1083/jcb.98.1.97

Keller, L.C., E.P. Romijn, I. Zamora, J.R. Yates III, and W.F. Marshall. 2005. Proteomic analysis of isolated *Chlamydomonas* centrioles reveals orthologs of ciliary-disease genes. *Curr. Biol.* 15:1090–1098. doi:10.1016/j.cub.2005.05.024

Kim, J.C., J.L. Badano, S. Sibold, M.A. Esmail, J. Hill, B.E. Hoskins, C.C. Leitch, K. Venner, S.J. Ansley, A.J. Ross, et al. 2004. The Bardet-Biedl protein BBS4 targets cargo to the pericentriolar region and is required for microtubule anchoring and cell cycle progression. *Nat. Genet.* 36:462–470. doi:10.1038/ng1352

Kim, J., S.R. Krishnaswami, and J.G. Gleeson. 2008. CEP290 interacts with the centriolar satellite component PCM-1 and is required for Rab8 localization to the primary cilium. *Hum. Mol. Genet.* 17:3796–3805. doi:10.1093/hmg/ddn277

Kindle, K.L. 1990. High-frequency nuclear transformation of *Chlamydomonas reinhardtii*. *Proc. Natl. Acad. Sci. USA.* 87:1228–1232. doi:10.1073/pnas.87.3.1228

King, S.M., T. Otter, and G.B. Witman. 1985. Characterization of monoclonal antibodies against *Chlamydomonas* flagellar dyneins by high-resolution protein blotting. *Proc. Natl. Acad. Sci. USA.* 82:4717–4721. doi:10.1073/pnas.82.14.4717

Lechtreck, K.F., and S. Geimer. 2000. Distribution of polyglutamylated tubulin in the flagellar apparatus of green flagellates. *Cell Motil. Cytoskeleton.* 47:219–235. doi:10.1002/1097-0169(200011)47:3<219::AID-CM5>3.0.CO;2-Q

Lechtreck, K.F., E.C. Johnson, T. Sakai, D. Cochran, B.A. Ballif, J. Rush, G.J. Pazour, M. Ikebe, and G.B. Witman. 2009. The *Chlamydomonas reinhardtii* BBSome is an IFT cargo required for export of specific signaling proteins from flagella. *J. Cell Biol.* 187:1117–1132. doi:10.1083/jcb.200909183

Leitch, C.C., N.A. Zaghloul, E.E. Davis, C. Stoetzel, A. Diaz-Font, S. Rix, M. Alfadhel, M. Al-Fadhel, R.A. Lewis, W. Eyaid, et al. 2008. Hypomorphic mutations in syndromic encephalocele genes are associated with Bardet-Biedl syndrome. *Nat. Genet.* 40:443–448. doi:10.1038/ng.97

Lumbreras, V., D.R. Stevens, and S. Purton. 1998. Efficient foreign gene expression in *Chlamydomonas reinhardtii* mediated by an endogenous intron. *Plant J.* 14:441–448. doi:10.1046/j.1365-313X.1998.00145.x

Maguire, A.M., F. Simonelli, E.A. Pierce, E.N. Pugh Jr., F. Mingozzi, J. Bennicelli, S. Banfi, K.A. Marshall, F. Testa, E.M. Surace, et al. 2008. Safety and efficacy of gene transfer for Leber's congenital amaurosis. *N. Engl. J. Med.* 358:2240–2248. doi:10.1056/NEJMoa0802315

McEwen, D.P., R.K. Koenekoop, H. Khanna, P.M. Jenkins, I. Lopez, A. Swaroop, and J.R. Martens. 2007. Hypomorphic *CEP290/NPHP6* mutations result in anosmia caused by the selective loss of G proteins in cilia of olfactory sensory neurons. *Proc. Natl. Acad. Sci. USA.* 104:15917–15922. doi:10.1073/pnas.0704140104

Nachury, M.V., A.V. Loktev, Q. Zhang, C.J. Westlake, J. Peränen, A. Merdes, D.C. Slusarski, R.H. Scheller, J.F. Bazan, V.C. Sheffield, and P.K. Jackson. 2007. A core complex of BBS proteins cooperates with the GTPase Rab8 to promote ciliary membrane biogenesis. *Cell.* 129:1201–1213. doi:10.1016/j.cell.2007.03.053

O'Toole, E.T., T.H. Giddings, J.R. McIntosh, and S.K. Dutcher. 2003. Three-dimensional organization of basal bodies from wild-type and delta-tubulin deletion strains of *Chlamydomonas reinhardtii*. *Mol. Biol. Cell.* 14:2999–3012. doi:10.1091/mbc.E02-11-0755

Pazour, G.J., O.A. Sineshchekov, and G.B. Witman. 1995. Mutational analysis of the phototransduction pathway of *Chlamydomonas reinhardtii*. *J. Cell Biol.* 131:427–440. doi:10.1083/jcb.131.2.427

Pazour, G.J., C.G. Wilkerson, and G.B. Witman. 1998. A dynein light chain is essential for the retrograde particle movement of intraflagellar transport (IFT). *J. Cell Biol.* 141:979–992. doi:10.1083/jcb.141.4.979

Pazour, G.J., B.L. Dickert, and G.B. Witman. 1999. The DHC1b (DHC2) isoform of cytoplasmic dynein is required for flagellar assembly. *J. Cell Biol.* 144:473–481. doi:10.1083/jcb.144.3.473

Pazour, G.J., N. Agrin, J. Leszyk, and G.B. Witman. 2005. Proteomic analysis of a eukaryotic cilium. *J. Cell Biol.* 170:103–113. doi:10.1083/jcb.200504008

Piasecki, B.P., and C.D. Silflow. 2009. The *UNI1* and *UNI2* genes function in the transition of triplet to doublet microtubules between the centriole and cilium in *Chlamydomonas*. *Mol. Biol. Cell.* 20:368–378. doi:10.1091/mbc.E08-09-0900

Piasecki, B.P., M. LaVoie, L.W. Tam, P.A. Lefebvre, and C.D. Silflow. 2008. The Uni2 phosphoprotein is a cell cycle regulated component of the basal body maturation pathway in *Chlamydomonas reinhardtii*. *Mol. Biol. Cell.* 19:262–273. doi:10.1091/mbc.E07-08-0798

Piperno, G., E. Siuda, S. Henderson, M. Segil, H. Vaananen, and M. Sassaroli. 1998. Distinct mutants of retrograde intraflagellar transport (IFT) share similar morphological and molecular defects. *J. Cell Biol.* 143:1591–1601. doi:10.1083/jcb.143.6.1591

Porter, M.E., R. Bower, J.A. Knott, P. Byrd, and W. Dentler. 1999. Cytoplasmic dynein heavy chain 1b is required for flagellar assembly in *Chlamydomonas*. *Mol. Biol. Cell.* 10:693–712.

Quarmby, L.M. 2009. Deflagellation. *In* The *Chlamydomonas* Sourcebook. Volume 3. G.B. Witman, editor. Academic Press/Elsevier, New York. 43–69.

Ringo, D.L. 1967. Flagellar motion and fine structure of the flagellar apparatus in *Chlamydomonas*. *J. Cell Biol.* 33:543–571. doi:10.1083/jcb.33.3.543

Rosenbaum, J.L., and G.B. Witman. 2002. Intraflagellar transport. *Nat. Rev. Mol. Cell Biol.* 3:813–825. doi:10.1038/nrm952

Sager, R., and S. Granick. 1953. Nutritional studies with *Chlamydomonas reinhardi*. *Ann. N. Y. Acad. Sci.* 56:831–838. doi:10.1111/j.1749-6632.1953.tb30261.x

Sayer, J.A., E.A. Otto, J.F. O'Toole, G. Nurnberg, M.A. Kennedy, C. Becker, H.C. Hennies, J. Helou, M. Attanasio, B.V. Fausett, et al. 2006. The centrosomal protein nephrocystin-6 is mutated in Joubert syndrome and activates transcription factor ATF4. *Nat. Genet.* 38:674–681. doi:10.1038/ng1786

Silflow, C.D., M. LaVoie, L.W. Tam, S. Tousey, M. Sanders, W. Wu, M. Borodovsky, and P.A. Lefebvre. 2001. The Vfl1 protein in *Chlamydomonas* localizes in a rotationally asymmetric pattern at the distal ends of the basal bodies. *J. Cell Biol.* 153:63–74. doi:10.1083/jcb.153.1.63

Stevens, D.R., J.D. Rochaix, and S. Purton. 1996. The bacterial phleomycin resistance gene *ble* as a dominant selectable marker in *Chlamydomonas*. *Mol. Gen. Genet.* 251:23–30.

Sundaresan, P., P. Vijayalakshmi, S. Thompson, A.C. Ko, J.H. Fingert, and E.M. Stone. 2009. Mutations that are a common cause of Leber congenital amaurosis in northern America are rare in southern India. *Mol. Vis.* 15:1781–1787.

Tam, L.W., W.L. Dentler, and P.A. Lefebvre. 2003. Defective flagellar assembly and length regulation in *LF3* null mutants in *Chlamydomonas*. *J. Cell Biol.* 163:597–607. doi:10.1083/jcb.200307143

Tamm, S.L. 1988. Iontophoretic localization of Ca-sensitive sites controlling activation of ciliary beating in macrocilia of Beroë: the ciliary rete. *Cell Motil. Cytoskeleton.* 11:126–138. doi:10.1002/cm.970110206

Tran, P.V., C.J. Haycraft, T.Y. Besschetnova, A. Turbe-Doan, R.W. Stottmann, B.J. Herron, A.L. Chesebro, H. Qiu, P.J. Scherz, J.V. Shah, et al. 2008. THM1 negatively modulates mouse sonic hedgehog signal transduction and affects retrograde intraflagellar transport in cilia. *Nat. Genet.* 40:403–410. doi:10.1038/ng.105

Tsang, W.Y., C. Bossard, H. Khanna, J. Peränen, A. Swaroop, V. Malhotra, and B.D. Dynlacht. 2008. CP110 suppresses primary cilia formation through its interaction with CEP290, a protein deficient in human ciliary disease. *Dev. Cell.* 15:187–197. doi:10.1016/j.devcel.2008.07.004

Valente, E.M., J.L. Silhavy, F. Brancati, G. Barrano, S.R. Krishnaswami, M. Castori, M.A. Lancaster, E. Boltshauser, L. Boccone, L. Al-Gazali, et al. 2006. Mutations in *CEP290*, which encodes a centrosomal protein, cause pleiotropic forms of Joubert syndrome. *Nat. Genet.* 38:623–625. doi:10.1038/ng1805

Weiss, R.L., D.A. Goodenough, and U.W. Goodenough. 1977. Membrane particle arrays associated with the basal body and with contractile vacuole secretion in *Chlamydomonas*. *J. Cell Biol.* 72:133–143. doi:10.1083/jcb.72.1.133

Witman, G.B. 1986. Isolation of *Chlamydomonas* flagella and flagellar axonemes. *Methods Enzymol.* 134:280–290. doi:10.1016/0076-6879(86)34096-5

Witman, G.B., K. Carlson, J. Berliner, and J.L. Rosenbaum. 1972. *Chlamydomonas* flagella. I. Isolation and electrophoretic analysis of microtubules, matrix, membranes, and mastigonemes. *J. Cell Biol.* 54:507–539. doi:10.1083/jcb.54.3.507

Wolff, A., B. de Néchaud, D. Chillet, H. Mazarguil, E. Desbruyères, S. Audebert, B. Eddé, F. Gros, and P. Denoulet. 1992. Distribution of glutamylated alpha and beta-tubulin in mouse tissues using a specific monoclonal antibody, GT335. *Eur. J. Cell Biol.* 59:425–432.